Available online at www.sciencedirect.com
ScienceDirect
Solar Energy xxx (2007) xxx–xxx
SOLAR ENERGY
www.elsevier.com/locate/solener

Comparison of modelling approaches and layouts for solar chimney turbines

T.P. Fluri *,[1], T.W. von Backström

Department of Mechanical Engineering, University of Stellenbosch, Private Bag X1, Stellenbosch 7602, South Africa

Received 18 September 2006; received in revised form 19 July 2007; accepted 20 July 2007

Communicated by: Associate Editor S.A. Sherif

Abstract

The turbogenerator is a core component of any solar chimney power plant. Various layouts for the turbogenerator have been proposed in the literature. In this paper the performance of these layouts is compared using analytical models and optimization techniques, and the important design parameters are discussed. The turbine layouts under consideration are single rotor and counter rotating turbines, both with or without inlet guide vanes.

In contrast to similar investigations found in the literature, various radial sections along the blades are analysed in the turbine model. This approach is more appropriate than using a simple mean line analysis when dealing with turbines with high blade aspect ratio and low hub to tip ratio. Furthermore, a limit to the degree of reaction of the turbine has been introduced to avoid diffusion at the hub.

It is shown in this paper that these slight changes in modelling approach have a significant impact on the performance prediction. Further it can be concluded that the single rotor layout without guide vanes performs very poorly; the efficiency of the other three layouts is much better and lies in a narrow band. The counter rotating layouts provide the highest peak efficiencies, but at relatively low speeds, which leads to an undesirable higher torque for the same power output.

Keywords: Solar chimney power plant; Turbogenerator layout; Performance modelling

1. Introduction

The main features of a solar chimney power plant are a solar collector and a tall chimney (Fig. 1). The collector consists of a circular transparent roof and the ground under the collector floor surface. Solar radiation heats the ground, which in turn heats the air under the collector roof like in a greenhouse. The hot air rises and escapes through the chimney. The resulting airflow is used to generate electricity via one or several turbogenerators. A pilot plant was built and tested in the 1980s in Manzanares, Spain. No full scale solar chimney power plant has been built to date. For the turbogenerators several layouts have been proposed in the solar chimney literature. The objective of this paper is the comparison of these layouts using various modelling approaches.

Schwarz and Knauss (1981) designed the turbogenerator for the pilot plant in Manzanares. For the turbine they chose a single rotor layout without guide vanes. Gannon and Von Backström (2002) proposed a single rotor layout for a large-scale solar chimney, in which they made use of the chimney support structure as inlet guide vanes. They present an analytical model for this layout, which is adapted from gas turbine literature, and show that the inlet guide vanes improve the performance (Von Backström and Gannon, 2004). They also point out that the values for specific speed and diameter for a solar chimney turbine lie between the ones of gas turbines and wind turbines.

* Corresponding author. Tel.: +27 218084281; fax: +27 218084958.
E-mail address: thomas.fluri@alumni.ethz.ch (T.P. Fluri).
[1] Supported by VolkswagenStiftung, Germany and the South African National Research Foundation.

0038-092X/$ - see front matter © 2007 Elsevier Ltd. All rights reserved.
doi:10.1016/j.solener.2007.07.006

Nomenclature

b_x	axial blade chord
c	nondimensional absolute flow velocity
c_h	blade chord
c_p	specific heat at constant pressure
C	absolute flow velocity
C_L	lift coefficient
d	diameter
h	enthalpy per unit mass flow
l_b	blade length
$\dot{m}$	mass flow
p	pressure
r	radius
R	specific gas constant
R_{asp}	blade aspect ratio
R_{HT}	hub to tip radius ratio
R_D	diffusor area ratio
R_n	degree of reaction
T	temperature
T_q	torque
u	nondimensional peripheral speed
U	peripheral speed
w	nondimensional relative flow velocity
W	relative flow velocity
Z	number of blades
Z_t	number of turbines
α	absolute flow angle
β	rotor relative flow angle
γ	ratio of specific heats
ϵ	flow deflection
η	efficiency
ρ	density
ζ	loss coefficient
Ψ	load coefficient
Φ	flow coefficient
σ	solidity
ω	rotational speed

Subscripts

a	first rotor
b	blade, second rotor
c	chimney
m	mean
op	optimum
t	tip, total condition
ts	total-to-static
tt	total-to-total, total turbine
u	circumferential
x	axial
0	upstream of inlet guide vanes
1	upstream of first rotor
2	downstream of first rotor
3	downstream of second rotor
4	downstream of diffuser

Abbreviations

CR	counter rotating
IGV	inlet guide vane
rpm	rotations per minute
SR	single rotor

More recently, Denantes and Bilgen (2006) introduced an alternative layout consisting of one pair of counter rotating rotors, either with or without inlet guide vanes. They modified the analytical model of Von Backström and Gannon (2004) to accommodate layouts with counter rotating rotors and to compare their performance to the one of the single rotor layout with inlet guide vanes. They find that the single rotor layout has a higher efficiency at the design point but a lower efficiency at off-design conditions.

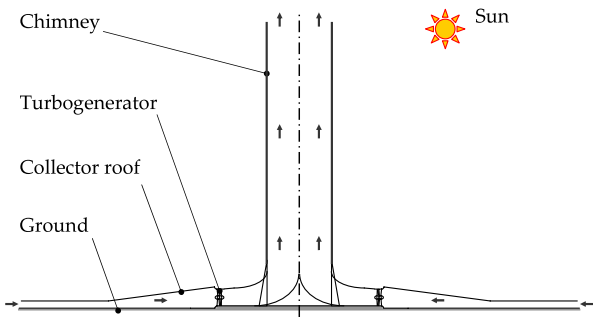

Fig. 1. Schematic drawing of a solar chimney power plant.

Denantes and Bilgen (2006) base their work on counter rotating turbines on earlier gas turbine and water turbine publications (Ozgur and Nathan, 1971; Louis, 1985; Cai et al., 1990). Ozgur and Nathan (1971) compare an axial flow counter rotating water turbine consisting of one rotor pair without inlet guide vanes to a single rotor turbine with inlet guide vanes. Louis (1985) compares two counter rotating layouts, both with one rotor pair but one with and one without inlet guide vanes, to single rotor layouts with inlet guide vanes. Cai et al. also look at axial counter rotating turbine layouts with or without guide vanes (Cai et al., 1990). In the earlier publications (Ozgur and Nathan, 1971; Louis, 1985) the rotational speed was assumed to be of equal magnitude for the two rotors and the flow was assumed to leave the turbine without swirl. In this study (Cai et al., 1990) a difference in rotor speed has been allowed for, and as an alternative to the zero exit swirl condition, layouts were studied where the exit swirl component is not zero but equal to the swirl component at the inlet. In the study of Denantes and Bilgen (2006) the speeds of the two rotors are also independent from each other and the exit swirl component is not limited to a certain value.

Please cite this article in press as: Fluri, T.P., von Backström, T.W., Comparison of modelling approaches and layouts for solar ..., Sol. Energy (2007), doi:10.1016/j.solener.2007.07.006

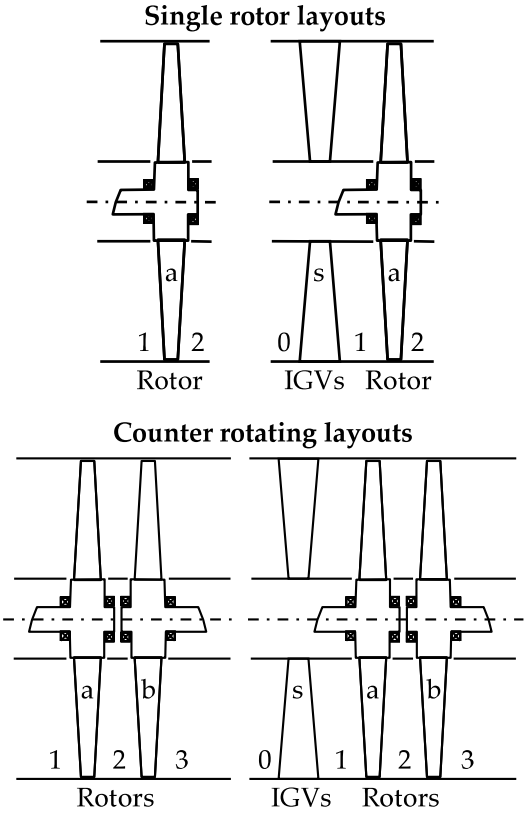

Fig. 2. Schematic drawing of turbine layouts.

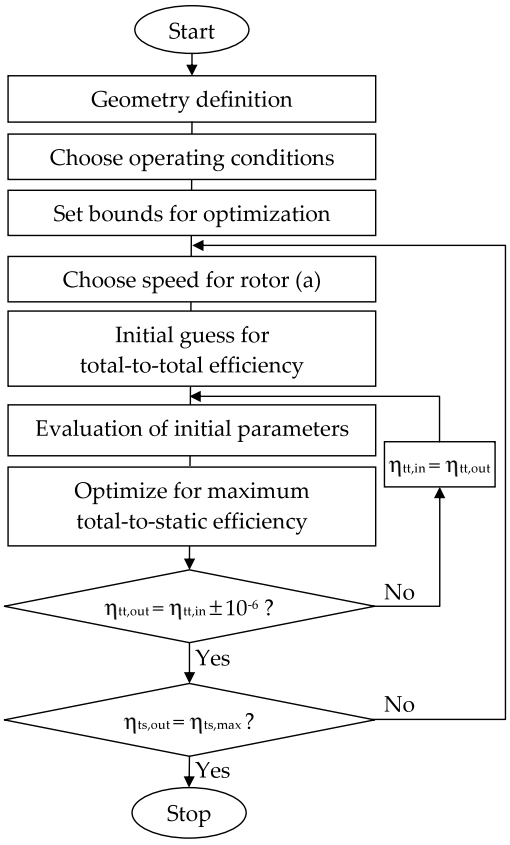

Fig. 3. Flow chart of algorithm.

A comparison based on Denantes and Bilgen (2006) is presented here, however, the evaluation of the turbine efficiency is modified (radial averaging is implemented, and secondary losses are taken into account), a limit to the turbine reaction is introduced to avoid diffusion at the hub, and the single rotor layout without inlet guide vanes is also considered.

For the comparison a multiple horizontal axis turbine configuration as shown in Fig. 1 is chosen here, and following the trends in the technology of large wind turbines, it is assumed that a variable speed drive train is used in all layouts (Bywaters et al., 2004; Poore and Lettenmaier, 2003). The turbine layouts considered in this paper are shown in Fig. 2.

2. Turbine modelling

2.1. Structure of the program

The program to enable the comparison of the layouts is structured as follows (Fig. 3):

(1) *Geometry definition.* The geometry of the flow passage and the turbine is defined. It is assumed that the diameter of the chimney is given and hence the chimney inlet area is known. The diffuser area ratio is defined as $R_D = A_c/A_{tt}$, where A_c is the chimney area and A_{tt} is the total turbine area. The number of turbines is specified. The blade aspect ratio, R_{asp}, and the hub-to-tip radius ratio, R_{HT}, are set.

(2) *Choose operating conditions.* The operating point and the working fluid are specified. The operating point is given with inlet total temperature, T_{t0}, inlet total pressure, p_{t0}, exit total pressure, p_{t4}, which is also the chimney inlet pressure, and mass flow, $\dot{m}$. The working fluid is assumed to be dry air. We assume incompressibility and the density is taken as $\rho = p_{t4}/(RT_{t0})$.

(3) *Set bounds for optimization.*

(4) *Choose speed for rotor (a).*

(5) *Initial guess.* An initial guess for the total-to-total turbine efficiency and the design variables, which will be defined in Section 2.2.1, is made.

(6) *Evaluation of initial parameters.* The axial components of the chimney inlet and the turbine exit flow velocities are

$$C_{x4} = \frac{\dot{m}}{A_c \rho} \tag{1}$$

$$C_{x3} = C_{x4} R_D \tag{2}$$

The static pressure at the exit and the temperature and enthalpy difference over the turbine are evaluated from

$$p_4 = p_{t4} - 0.5\rho C_{x4}^2 \tag{3}$$

$$\Delta T = \eta_{tt} T_{t0}\left(1 - \left(\frac{p_{t1}}{p_{t4}}\right)^{\frac{\gamma}{\gamma-1}}\right) \tag{4}$$

$$\Delta h = c_p \Delta T \tag{5}$$

The stage load coefficient Ψ and flow coefficient Φ can be evaluated from

$$\Psi = \frac{\Delta h}{U_a^2} \tag{6}$$

where U_a is the absolute blade speed of the first rotor, and

$$\Phi = \frac{C_x}{U_a} \tag{7}$$

(7) *Optimize for total-to-static efficiency.* Utilizing the specific turbine model, which will be described in detail below, an optimization algorithm is run to get the maximum total-to-static efficiency at this particular speed of the first rotor. As long as the total-to-total efficiency value has not converged we iterate. At each iteration the efficiency result is taken as the new initial guess. The optimization algorithm used here is the function "fmincon", which is the Sequential Quadratic Programming implementation for constrained optimization in Matlab.

(8) *Detect optimal speed of rotor (a).* The above iteration is executed with new values for the speed of rotor (a), until the speed providing the maximum total-to-static efficiency has been detected.

2.2. Mathematical turbine models

The model for the counter rotating layout with inlet guide vanes is described in detail here. It serves as a basis for all the other models. Having three blade rows, it is the most complex one, and the others can be derived from it by simply deleting one or two blade rows and their impact on the flow (Fig. 2). The model has been adapted from the work of Denantes and Bilgen (2006).

2.2.1. Velocity diagram

Some assumptions:

- The mass flow is equally shared by the various turbines.
- No turbine flare.
- Constant axial velocity through turbine: $C_x = C_{x1} = C_{x2} = C_{x3}$.
- Zero swirl at turbine inlet: $C_{u0} = 0$.
- Free vortex design.

The design variables for the optimization are the dimensionless blade speed of the second rotor $u_b = U_b/U_a$, the degree of reaction of the first rotor

$$R_{n,a} = 1 - (c_{u2} + c_{u1})/2 = -(w_{u2a} + w_{u1})/2 \tag{8}$$

and the degree of reaction of the second rotor

$$R_{n,b} = 1 - \frac{c_{u3} + c_{u2}}{2u_b} = -\frac{w_{u3} + w_{u2b}}{2u_b} \tag{9}$$

The small letters c and w denote dimensionless absolute and relative flow velocities respectively and the subscript u indicates the circumferential direction.

The degree of reaction, represents the ratio of the static pressure drop to the stagnation pressure drop over a turbine rotor (Wilson and Korakianitis, 1998). The above equations can be derived using the Euler equation, the velocity diagram (see Fig. 4) and assuming the axial component of the flow velocity to be equal at rotor inlet and outlet. For a derivation of Eq. (8) refer to (Von Backström and Gannon, 2004). Denantes and Bilgen (2006) use a slightly different parameter for the second rotor, which is equal to the actual degree of reaction multiplied by u_b. The load coefficients are defined as follows:

Stage load coefficient:

$$\Psi = c_{u1} - c_{u2} + u_b(c_{u2} - c_{u3}) \tag{10}$$

Load coefficient of the first rotor:

$$\Psi_a = c_{u1} - c_{u2} \tag{11}$$

Load coefficient of the second rotor:

$$\Psi_b = u_b(c_{u2} - c_{u3}) \tag{12}$$

Using these definitions and some algebraic manipulations we get the following dimensionless velocity components:

$$c_{u1} = 1 - R_{n,a} + \Psi_a/2 \tag{13}$$

$$w_{u1} = c_{u1} - 1 = -R_{n,a} + \Psi_a/2 \tag{14}$$

$$c_{u2} = 1 - R_{n,a} - \Psi_a/2 \tag{15}$$

$$w_{u2,a} = c_{u2} - 1 = -R_{n,a} - \Psi_a/2 \tag{16}$$

$$c_{u2} = u_b(1 - R_{n,b}) + \frac{\Psi_b}{2u_b} \tag{17}$$

$$w_{u2,b} = c_{u2} - u_b = -u_b R_{n,b} + \frac{\Psi_b}{2u_b} \tag{18}$$

$$c_{u3} = u_b(1 - R_{n,b}) - \frac{\Psi_b}{2u_b} \tag{19}$$

$$w_{u3} = c_{u3} - u_b = -u_b R_{n,b} - \frac{\Psi_b}{2u_b} \tag{20}$$

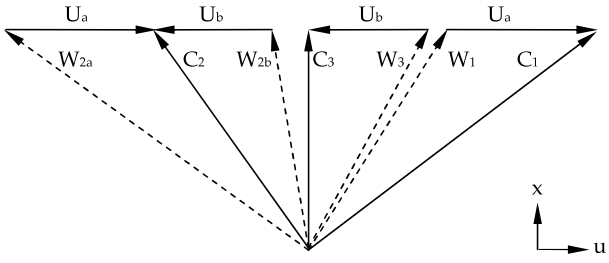

Fig. 4. Velocity triangles of a counter rotating turbine stage with inlet guide vanes (similar to Denantes and Bilgen, 2006 but without diffusion in blade rows).

Using Pythagoras's relations we can now evaluate all the flow angles and velocity components similar to the following two examples, the stator exit flow angle and the dimensionless stator exit velocity squared:

$$\alpha_1 = \arctan\frac{c_{u1}}{\Phi} \tag{21}$$

$$c_1^2 = \Phi^2 + c_{u1}^2 \tag{22}$$

Assuming that the swirl remains constant from the exit of the turbine to the chimney inlet,[2] the flow velocity at the chimney inlet is obtained from:

$$c_4^2 = c_{x4}^2 + c_{u3}^2 \tag{23}$$

Equating (15) in (17) gives

$$\Psi_b = 2u_b(1 - R_{n,a} - \Psi_a/2 - u_b(1 - R_{n,b})) \tag{24}$$

and with $\Psi = \Psi_a + \Psi_b$

$$\Psi_a = \frac{\Psi - 2u_b(1 - R_{n,a} - u_b(1 - R_{n,b}))}{1 - u_b} \tag{25}$$

With this a model has been obtained, which depends only on the three design variables and on the chosen turbine speed and operating conditions.

2.2.2. Losses and efficiency

For profile losses Hawthorne's simplification of Soderberg's correlation is implemented, where ϵ denotes the flow deflection (Horlock, 1966):

$$\zeta_p = 0.025\left(1 + \left(\frac{\epsilon}{90^\circ}\right)^2\right) \tag{26}$$

Hawthorne also gives a correlation for secondary loss implying it to be proportional to the profile loss and the blade aspect ratio:

$$\zeta_{sec} = \zeta_p\frac{3.2}{R_{asp}} \tag{27}$$

The blade aspect ratio is taken as $R_{asp} = l_b/b_x$ where l_b is the blade length and b_x is the axial chord of the blade. Adding the secondary to the profile loss and neglecting tip leakage and annulus losses the overall loss coefficient for a single blade row becomes:

$$\zeta = 0.025\left(1 + \left(\frac{\epsilon}{90^\circ}\right)^2\right)\left(1 + \frac{3.2}{R_{asp}}\right) \tag{28}$$

This loss model has been employed by many authors, (e.g. Gannon and Von Backström, 2002), while others chose to neglect secondary losses, (e.g. Von Backström and Gannon, 2004; Denantes and Bilgen, 2006).

Since the total-to-static efficiency is the appropriate measure of performance for a solar chimney turbine the following equation is included into the model:

$$\eta_{ts} = \frac{1}{1 + \frac{\zeta_s c_1^2 + \zeta_a w_{2a}^2 + \zeta_b w_3^2 + c_4^2}{2\Psi}} \tag{29}$$

The total-to-total efficiency can be assessed from

$$\eta_{tt} = \frac{1}{1 + \frac{\zeta_s c_1^2 + \zeta_a w_{2a}^2 + \zeta_b w_3^2}{2\Psi}} \tag{30}$$

The loss coefficients and the relative velocities are evaluated at seven equally spaced radial stations along the span of the blades and the final value of the efficiencies is area-averaged.

2.2.3. Torque evaluation

The torque on the rotors is assessed from $T_q = P/\omega$, where P is the power and ω is the rotational speed. The power is evaluated from the well-known Euler turbine equation. The rotational speed can be written as $\omega = U/r$. Combining the above gives the following equations for the torque:

$$T_{q,a} = \dot{m}U_a r_m(c_{u1} - c_{u2}) \tag{31}$$

$$T_{q,b} = \dot{m}U_a r_m(c_{u2} - c_{u3}) \tag{32}$$

2.2.4. Solidity and number of blades

Implementing the above loss model it is assumed that the turbine operates near optimum solidity. With the flow angles, the blade aspect ratio, the hub-to-tip radius ratio and the through flow area given, the number of blades is the only free parameter controlling the solidity.

According to Wilson and Korakianitis (1998) minimum-loss solidities are found by setting the tangential lift coefficient, C_L, at a constant value between 0.8 and 1.2. In the following the optimum lift coefficient is assumed to be equal to unity. The optimum axial solidity can be found using their equation 7.5, which is reiterated here for convenience

$$\left(\frac{b_x}{s}\right)_{op} = \left|\frac{2}{C_{L,op}}\cos^2\alpha_{ex}(\tan\alpha_{in} - \alpha_{ex})\right| \tag{33}$$

b_x is the axial blade chord, s is the spacing between the blades and α_{in} and α_{ex} are the flow angles at blade row inlet and outlet. The axial chord of the blade can be approximated with

$$b_x = c_h\cos\left(\frac{\alpha_{in} + \alpha_{ex}}{2}\right) \tag{34}$$

where c_h is the actual blade chord and the fraction denotes an average flow angle through the blade row. The blade chord is obtained by dividing the blade length, l_b, by the blade aspect ratio, R_{asp}. The optimum number of blades can then be obtained from

$$Z = 2\pi r_m\frac{(b_x/s)_{op}}{b_x} \tag{35}$$

[2] This does not represent the real situation, but whether the swirl component is lost through friction or as exit loss at the chimney top, its effect on the turbine performance is the same.

Please cite this article in press as: Fluri, T.P., von Backström, T.W., Comparison of modelling approaches and layouts for solar ..., Sol. Energy (2007), doi:10.1016/j.solener.2007.07.006

2.2.5. Constraints

The degree of reaction of a free-vortex turbine stage changes along the blade. The lowest degree of reaction is found at the hub and the highest at the tip. To avoid recompression at the hub, which would most probably lead to flow separation and performance deterioration, the reaction should not be less than that of an impulse stage, which is zero. The effect of this constraint, which has been ignored by other authors, is investigated here.

2.2.6. Models for layouts two, three and four

As mentioned above, the models of the other three layouts can be derived from the one presented above by deleting blade rows and their impact on the flow. To model a turbine without inlet guide vanes both the absolute flow angle at the stator exit, α_1, and the stator loss coefficient, ζ_S, are set to zero (Denantes and Bilgen, 2006). Modelling a single rotor turbine, two design variables, the reaction and the dimensionless speed of the second rotor, $R_{n,\mathrm{b}}$ and u_b, fall away. The loss coefficient of the second rotor, ζ_b, is set to zero, and the circumferential component of the turbine exit velocity, c_{u3}, is set equal to c_{u2}, the circumferential component of the exit velocity of the first rotor.

3. Comparison of layouts

For a first comparison the geometrical parameters, the operating conditions and the assumed values for the fluid properties are shown in Table 1. The operating conditions have been extracted from (Von Backström and Gannon, 2004).

3.1. Efficiency

Fig. 5 shows the efficiency prediction for the various turbine layouts over a range of turbine speeds. Most obviously the single rotor layout without inlet guide vanes is not able to reach an acceptable total-to-static efficiency at any speed, with its peak lying at a 66.9%, making either a stator or an additional rotor row inevitable. The peak total-to-static efficiency of the other three layouts lies in a narrow band between 79.6 (SR with IGVs) and 80.1% (CR with IGVs). However, the speed of the first rotor at which these three layouts reach their peak efficiency varies a lot. The single rotor turbine performs very poorly at low speeds, mainly due to high exit losses resulting from a high exit swirl, which is necessary to prevent diffusion at the hub. It performs best at 29.2 rpm. Going to higher speeds, the performance deteriorates mainly due to high rotor losses resulting from high relative flow velocities.

Table 1
Geometrical parameters and operating conditions

Chimney height	H_C (m)	1500
Chimney diameter	d_C (m)	160
Collector outer diameter	d_col (m)	6000
Number of turbines	Z_t	32
Diffuser area ratio	R_D	1.0
Stator blade aspect ratio	$R_\mathrm{asp,s}$	4.0
Rotor blade aspect ratio	$R_\mathrm{asp,r}$	3.0
Hub-to-tip radius ratio	R_HT	0.4
Inlet total pressure	p_t0 (Pa)	90,000
Inlet total temperature	T_t0 (K)	333
Exit total pressure	p_t4 (Pa)	89,200
Mass flow rate	$\dot{m}$ (ton/s)	250
Specific gas constant	R (J/kg)	287
Specific heat at constant pressure	c_p (J/(kg K))	1008
Ratio of specific heats	γ	1.4

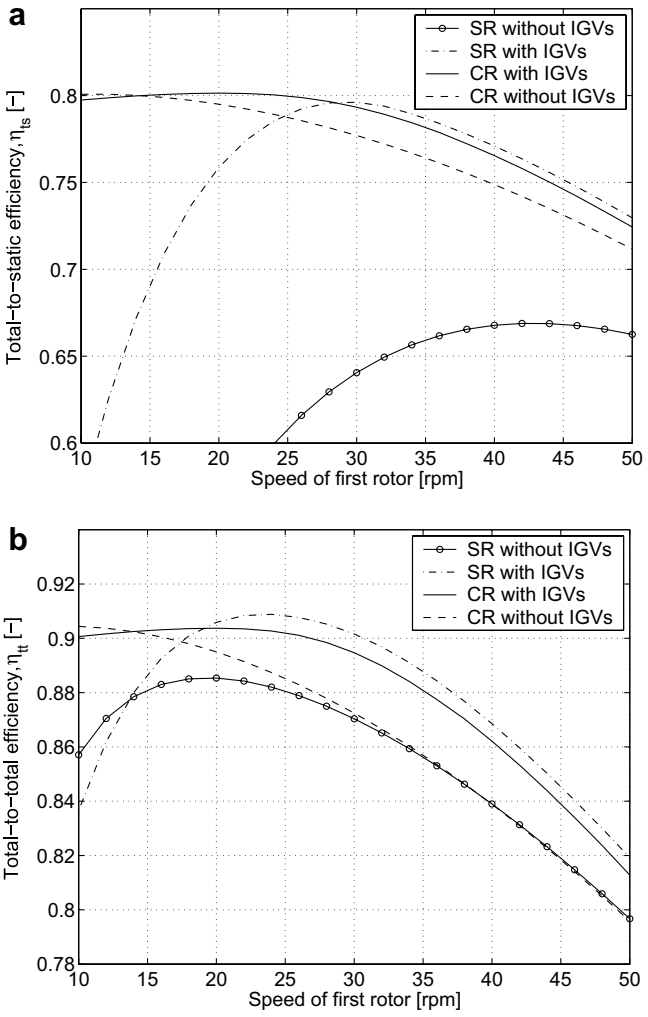

Fig. 5. (a) Total-to-static and (b) total-to-total efficiency prediction for various layouts for a single axial turbine stage.

The counter rotating turbine with inlet guide vanes suffers from the same effect if the first rotor runs faster than at 20 rpm, which is the optimum speed of this layout for the given geometric parameters and operating conditions. Pushing the first rotor to higher speeds, the optimizer slows down the second rotor significantly (Fig. 6). The lower limit of the dimensionless speed of the second rotor has been set to a 10th of the first rotor's speed ($u_\mathrm{b,min} = -0.1$). This limit is reached at a speed of 38 rpm of the first rotor. For speeds lower than the optimum, the performance deteriorates only slightly, since the exit swirl does not increase a lot.

Please cite this article in press as: Fluri, T.P., von Backström, T.W., Comparison of modelling approaches and layouts for solar ..., Sol. Energy (2007), doi:10.1016/j.solener.2007.07.006

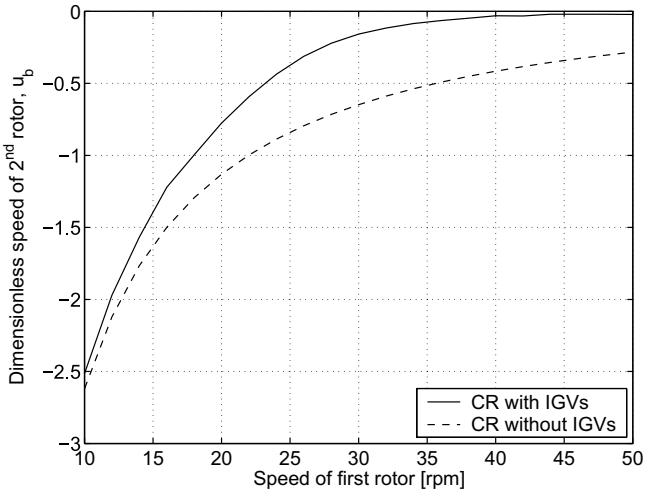

Fig. 6. Dimensionless speed of the second rotor vs. turbine speed.

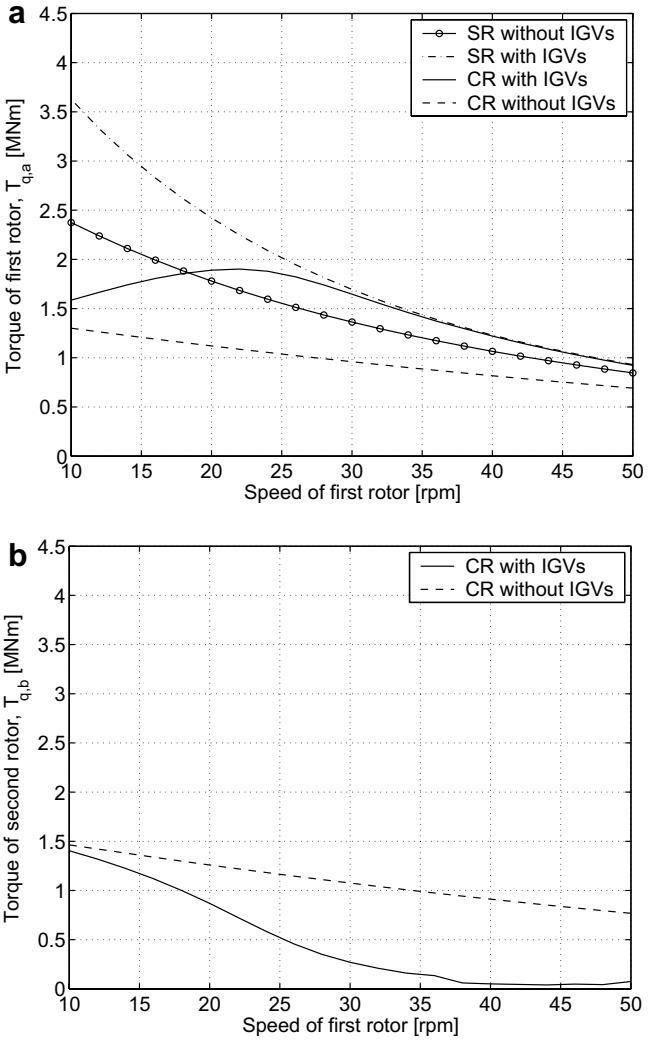

Fig. 7. Torque on first (a) and second rotor (b) for various layouts for a single axial turbine stage.

The counter rotating turbine without inlet guide vanes follows a similar trend as the previous layout, but its peak is shifted to the low speed side resulting in a high torque for high performance (Fig. 7).

3.2. Torque

Size and cost of the drive train is proportional to the torque delivered by the turbine. Since the power is proportional to the product of the rotational speed ω and the torque T_q, speeding up the turbine obviously reduces the torque for the same power output (Fig. 7). Since the performance peaks of the counter rotating layouts lie at relatively low speed the torque on the shafts is high, leading to a bigger and more expensive drive train.

This is very pronounced without IGVs with a torque of 1.28 and 1.45 MN m for the two shafts respectively. With IGVs the torque is slightly higher in the first rotor (1.35 MN m) but lower in the second rotor (0.87 MN m). Even though the single rotor solution with IGVs has only one rotor to carry all the load, the torque at peak performance is relatively low (1.74 MN m) thanks to the high speed. The torque for the rotor-only layout follows a similar trend but on a lower level due to the lower efficiency.

3.3. Solidity and number of blades

The required number of blades is obviously highly dependent on the chosen blade aspect ratio. With the parameters chosen here, results are as follows: besides the rotor-only layout, which requires only six blades, the layout with the lowest number of blades is the counter rotating turbine without IGVs, requiring 32 blades in its peak performance point (0 for the stator/16 for the first/16 for the second rotor). The single rotor layout requires 47 (31/16/0) and the counter rotating turbine with IGVs 66 blades (32/18/16).

4. Comparison of various modelling approaches

The main difference between the turbine model presented here and earlier models of other researchers are the implementation of a model for secondary losses, averaging over several radial sections for efficiency evaluation and the constraint on reaction to prevent diffusion at the hub. In Table 2 the results obtained with the current model are compared to simulations where one or all of the above features of the model have been removed. The efficiency is generally higher for the simpler models—8.5% points for the rotor-only layout and approximately 6% points for the other three layouts, if all of the above features have been removed—and the optimum rotor speed is significantly shifted. Neglecting the secondary losses has the biggest impact on the efficiency.

Removing the constraint on the degree of reaction has only a slight impact but does not affect all layouts in the same way: it has no impact on the rotor-only layout but increases the peak efficiency estimates of the three other

Please cite this article in press as: Fluri, T.P., von Backström, T.W., Comparison of modelling approaches and layouts for solar ..., Sol. Energy (2007), doi:10.1016/j.solener.2007.07.006

Table 2
Turbine parameters for various layouts and modelling approaches—Model 1: current model; Model 2: no constraint preventing recompression at the hub; Model 3: no radial averaging; Model 4: no secondary loss model; Model 5: models 2, 3, and 4 combined

Model		Single rotor		Counter rotating	
		No IGVs	With IGVs	No IGVs	With IGVs
1	η_{ts} (%)	66.9	79.6	80.1	80.1
	N_a (rpm)	42.8	29.2	10.9	20.0
	u_b	n/a	n/a	−2.35	−0.77
2	η_{ts} (%)	66.9	80.2	81.0	80.7
	N_a (rpm)	42.8	25.4	11.4	15.6
	u_b	n/a	n/a	−1.63	−0.95
3	η_{ts} (%)	69.4	82.7	82.8	82.6
	N_a (rpm)	45.8	32.1	7.5	26.0
	u_b	n/a	n/a	−3.84	−0.31
4	η_{ts} (%)	73.3	83.6	84.1	84.2
	N_a (rpm)	53.1	31.3	12.9	19.8
	u_b	n/a	n/a	−2.09	−0.93
5	η_{ts} (%)	75.4	86.0	86.2	86.0
	N_a (rpm)	56.8	33.8	7.8	23.1
	u_b	n/a	n/a	−3.89	−0.66

layouts, but not to the same extent with each of them. This could induce a bias towards certain layouts.

5. Conclusions

It has been shown that slight changes in the modelling of solar chimney turbines have a significant impact on the performance prediction. Neglecting secondary losses, for example, may lead to a significant overestimation of the turbine efficiency. Ignoring the constraint of recompression in the blade row, on the other hand, does not affect all layouts in the same way, which could lead to bad choices early in the preliminary phase of a large-scale solar chimney project.

It has also been found that the rotor-only layout is the simplest and cheapest layout requiring comparably few blades and a small drive train. Its total-to-static efficiency is very low, however, because the swirl at the turbine exit cannot be recovered. For the three other layouts the maximum total-to-static efficiency is much better and lies in a narrow band with the counter rotating turbines performing slightly better, however only at low speeds, which leads to a higher torque for the same power output.

In future work the model presented here can be linked to a cost model, in order to assess which layout provides the lowest cost of electricity.

References

Bywaters, G., John, V., Lynch, J., Mattila, P., Norton, G., Stowell, J., Salata, M., Labath, O., Chertok, A., Hablanian, D., 2004. Northern Power Systems WindPACT drive train alternative design study report, Tech. Rep. NREL/SR-500-35524, National Renewable Energy Laboratory, Colorado, revised October 2004.

Cai, R., Wu, W., Fang, G., 1990. Basic analysis of counter-rotating turbines, in: Proceedings of the 35th International Gas Turbine and Aeroengine Congress and Exposition, ASME.

Denantes, F., Bilgen, E., 2006. Counter-rotating turbines for solar chimney power plants. Renewable Energy 31, 1873–1891.

Gannon, A.J., Von Backström, T.W., 2002. Solar chimney turbine part 1 of 2: Design, in: International Solar Energy Conference, pp. 335–341.

Horlock, J.H., 1966. Axial Flow Turbines – Fluid Mechanics and Thermodynamics. Butterworths, London.

Louis, J.F., 1985. Axial flow contra-rotating turbines, in: Proceedings of the 30th International Gas Turbine Conference and Exhibit, ASME, Houston.

Ozgur, C., Nathan, G., 1971. A study of contrarotating turbines based on design efficiency. Journal of Basic Engineering 93, 395–404.

Poore, R., Lettenmaier, T., 2003. WindPACT Advanced wind turbine drive train designs study, Tech. Rep. NREL/SR-500-33196, National Renewable Energy Laboratory, Colorado.

Schwarz, G., Knauss, H., 1981. Strömungstechnische Auslegung des Aufwindkraftwerks Manzanares (Aerodynamic design of the solar chimney power plant in Manzanares), Tech. rep., Institut für Aerodynamik, Unversität Stuttgart, (in German).

Von Backström, T.W., Gannon, A.J., 2004. Solar chimney turbine characteristics. Solar Energy 76, 235–241.

Wilson, D.G., Korakianitis, T., 1998. The Design of High-Efficiency Turbomachinery and Gas Turbines, 3rd ed. Prentice Hall, London.

Please cite this article in press as: Fluri, T.P., von Backström, T.W., Comparison of modelling approaches and layouts for solar ..., Sol. Energy (2007), doi:10.1016/j.solener.2007.07.006